

Adsorption of different dyes from aqueous solution using Si-MCM-41 having very high surface area

Haribandhu Chaudhuri¹ · Subhajit Dash¹ · Ashis Sarkar¹

Published online: 16 April 2016
© Springer Science+Business Media New York 2016

Abstract Adsorption characteristics of four different dyes Safranin O (cationic), Neutral Red (neutral), Congo Red (anionic) and Reactive Red 2 (anionic) on Si-MCM-41 material having very high surface area are reported. The surface morphology of Si-MCM-41 material before and after adsorbing dye molecules are characterised by FTIR, HRXRD, nitrogen adsorption–desorption isotherms, FESEM, and HRTEM. The adsorption capacities of Si-MCM-41 for the dyes followed a decreasing order of NR > SF > CR > RR2. The adsorption kinetics, isotherm and thermodynamic parameters are investigated in detail for these dyes using calcined Si-MCM-41. The kinetics and isotherm data showed that both SF and NR adsorb more rapidly than CR and RR2, in accordance with pseudo-second-order kinetics model as well as intraparticle diffusion kinetics model and Langmuir adsorption isotherm model respectively. The thermodynamic data suggest that the dye uptake process is spontaneous. The high adsorption capacities of dyes on Si-MCM-41 ($q_m = 275.5 \text{ mg g}^{-1}$ for SF, $q_m = 288.2 \text{ mg g}^{-1}$ for NR) is explained on the basis of electrostatic interactions as well as H-bonding interactions between adsorbent and adsorbate

molecules. Good regeneration capacity is another important aspect of the material that makes it potent for the uptake of dyes from aqueous solution.

Keywords Si-MCM-41 · Different dyes · Adsorption · Interactions

List of symbols

q_m	Adsorption capacity
M_w	Molecular weight
C_0 and C_e	Initial and equilibrium concentrations of adsorbate solutions (mg L^{-1})
V	The volume of the dye solution
W	The weight of the adsorbent
$E = hv$	Plank equation
S	The pore size dependent on the assumed pore geometry
V_p	The mesoporous volume
ρ	The pore wall density (i.e. $2.2 \text{ cm}^3/\text{g}$ for siliceous materials)
d	The XRD interplanar spacing
R^2	Correlation coefficient
χ^2	Correction factor
R_L	Separation factor
ΔG°	The change in Gibbs free energy (J Mol^{-1})
ΔH°	The change in enthalpy (J Mol^{-1})
ΔS°	The change in entropy ($\text{J Mol}^{-1} \text{ K}^{-1}$)

Electronic supplementary material The online version of this article (doi:10.1007/s10934-016-0181-4) contains supplementary material, which is available to authorized users.

✉ Ashis Sarkar
a_sarkar_99@yahoo.com

Haribandhu Chaudhuri
chaudhuri.haribandhu@gmail.com

Subhajit Dash
subhajit.dash@gmail.com

¹ Organic Materials Research Laboratory, Department of Applied Chemistry, Indian School of Mines, Dhanbad, Jharkhand 826004, India

1 Introduction

Environmental pollution plays vital impact on everyday life. There are some toxic chemicals which are discharged into the environment as industrial wastes, having

dangerous effects on water, air, and soil. The pollution is occurring due to the mismanagement of contaminated water. A huge amount of water pollution comes from textile industry [1, 2]. Dyes are widely used in many industrial fields such as textiles, coatings, rubber, plastics etc. Apart from dyes causing water pollution, their degradation products may be toxic to human beings and also other animals [3–8]. There are various techniques of dye removal and many studies have been carried out to pay attention for adsorption technologies to remove dyes from aqueous solution [9, 10]. It is already established that the water treatment of dyes has a good application of adsorption process using suitable adsorbent and for that purpose highly porous materials are generally used [11, 12]. Besides this, an interest is developed for new recyclable adsorbents which very efficiently remove organic–inorganic pollutants from aqueous solution. The application of adsorption technology utilizing commercial activated carbon has become well known to remove effluents of dyes [13, 14]. However, activated carbon often suffers from high-cost of production and regeneration. Therefore, other materials such as some natural adsorbents (e.g., clays and clay minerals, cellulosic materials, chitins), waste materials, and some agricultural by-products are alternative adsorbents [15–21]. Various adsorbents including clays [22], zeolites [23], magnetic dendritic materials [24–26], polymeric materials [27], organically modified clays [28], layered double hydroxides [29], and mesoporous silica [23, 30, 31] have been used in the removal of dyes from aqueous solution.

In this context, high surface area and nano-meter sized mesoporous materials especially Si-MCM-41 can serve as a special environment for chemical separations of large molecules (such as dyes) [32]. It is also used for testing various adsorptions and desorption studies of its high pore volume. The interesting part of these materials is that the adsorbent and the adsorbate can be regenerated by simple washing with acid or basic solutions [33, 34].

In the present study, our objective is to examine the plausible effect of interactions among various dyes with surface active sites of the adsorbent and the potential of Si-MCM-41 for the removal of dyes from aqueous solution by measuring the adsorption data of four dyes such as Safranin O (Basic Red 2, SF), Neutral Red (Basic Red 5, NR), Congo Red (Sodium salt of 3,3'-([1,1'-biphenyl]-4,4'-diyl)bis(4-aminonaphthalene-1-sulfonic acid, CR)) and Reactive Red 2 (Red MX-5B, RR2). SF is also used for biological staining. NR is generally used for staining in histology and also some growth medium for bacterial and cell culture. CR, a known human carcinogen and mutagen, is a potential danger for bioaccumulation and can cause allergic problems [35, 36]. RR2 is mainly used for cotton, wool, silk and knot dyeing. The changes of surface

characteristics and pore structure of Si-MCM-41 introduced by those dye adsorption were characterized based on the analyses of the Fourier transform infrared (FTIR) spectra, the high resolution X-ray diffraction (HRXRD) patterns, the nitrogen adsorption isotherms, field emission scanning electron microscopy (FESEM) and high resolution transmission electron microscopy (HRTEM). The interactions between the groups present on the surface of Si-MCM-41 and with the groups present in those corresponding dyes were discussed. Moreover, for dye with high adsorption capacity, the adsorption processes with respect to pH, contact time, temperature, adsorbent dose, and dye concentration were also measured to provide more information about the adsorption characteristics of Si-MCM-41. The thermodynamic and kinetic parameters were calculated to determine the adsorption mechanism. The equilibrium data were fitted into Langmuir, Freundlich and Temkin equations to determine the correlation between the experimental data and the isotherm models.

2 Experimental

2.1 Materials

Tetraethoxysilane (TEOS, $\geq 99\%$) was purchased from Sigma Aldrich. CTAB ($(C_{16}H_{33})N(CH_3)_3Br$, $M_w = 364.45$) was obtained from Acros Organics. Triethanolamine (TEA, $N(CH_2CH_2OH)_3$, $\geq 98\%$) was purchased from S. D. fine-chem. Ltd and ethanol (EtOH, $\geq 99\%$) was purchased from Merck India. Deionised water was used without further purification. SF, NR, CR and RR2 were selected as adsorbates to determine the adsorption selectivity of Si-MCM-41 in terms of pore structure of adsorbents and molecular shape of adsorbates. These dyes of analytical grade were purchased from Loba Chemie and used without further purification. The structures of these dyes are presented in Fig. 1.

2.2 Preparation of Si-MCM-41

The mesoporous Si-MCM-41 material was prepared by a method where TEOS was added into aqueous solution containing CTAB, ethanol, some amount of additive agents like TEA. The synthesis of the material was carried out following an earlier report [37]. In a typical procedure, 6.4 mL of water (0.36 mol), 0.9 g of ethanol (0.015 mol), 1.04 g of a 25 wt% CTAB solution (0.786 mmol), and 0.02 g of TEA (0.19 mmol) were mixed and stirred in an oil bath at 60 °C for 45 min. 0.73 mL of TEOS (3.25 mmol) was added into the mixture dropwise within 2 min. with stirring. The solution turned white gradually. A further 2 h of stirring was necessary. Then, the solution

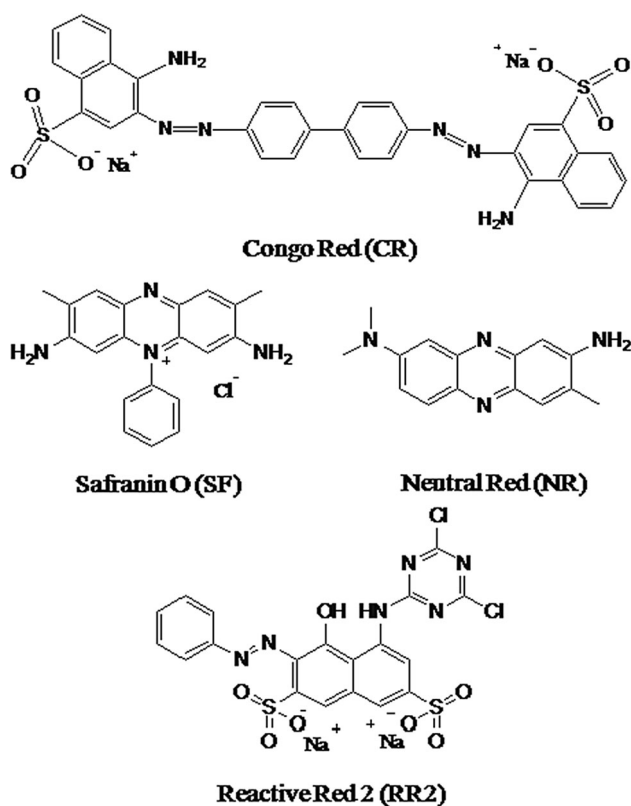


Fig. 1 Chemical structures of dyes used for adsorption

was cooled to room temperature and the solid product was filtered, washed with deionised water, distilled ethanol and air-dried overnight. Finally, the material was calcined at 550 °C for 6 h.

2.3 Measurements

2.3.1 Adsorption measurements

SF, NR, CR, and RR2 were first dried at 115 °C for 24 h to remove moisture before use. All of the dye solutions were prepared with deionised water. For adsorption experiments, the pH of the solution was adjusted with the help of HCl or NaOH solution to maintain a constant value. The dye adsorption study was performed (for SF, NR, CR, and RR2 respectively for the adsorption experiments to reach equilibrium) using an orbital shaker (Rivotek, Kolkata, India). After centrifugation at 3000 rpm for 20 min. in a REMI R-8C centrifuge, the mixture was left undisturbed overnight. After that, it was filtered and 20 mL of the solution was analysed for SF, NR, CR, and RR2 by UV-2450 (Shimadzu, Japan) at the wavelength (λ_{maxes}) of 518, 529, 499 and 489 nm respectively. The studies of pH variation, contact time, temperature variation, initial dye concentration and

adsorbent dosage were carried out according to the previously reported procedure [38]. For all study, 25 mL dye solutions were used. The effects of temperature and pH on the adsorption data were carried out by performing the adsorption experiments at various temperatures (25–60 °C) and various pH (2–9) respectively. The percent dye adsorption was calculated by using Eq. 1 [38].

$$\% \text{Adsorption} = \frac{C_0 - C_e}{C_e} \times 100 \quad (1)$$

The equilibrium uptake was calculated by using Eq 2 [38, 39],

$$q_e = (C_0 - C_e) \times \frac{V}{W} \quad (2)$$

where q_e represents equilibrium capacity of dye on Si-MCM-41 (mg g^{-1}), C_0 and C_e are the initial and equilibrium concentrations of adsorbate solutions (mg L^{-1}), respectively. V denotes the volume of the dye solution (L) used and W is the weight of the adsorbent (g) used. The results shown here are the arithmetic means of three experiments. For the experiment of adsorption kinetics, the dye adsorption amounts were determined by analysing the solution at appropriate time intervals.

2.3.2 Desorption measurements

The regenerability of the material was determined in three subsequent adsorption–desorption cycles. Desorption measurements were carried out in the same way as depicted earlier [38]. Dyes were adsorbed on the adsorbent by the method described above. Then, the adsorbent was treated with an aqueous solution to desorb the dye on the adsorbent. The aqueous solutions for the desorption experiments were prepared by adjusting of pH of deionized water at pH 2, 7, or 9 with dilute NaOH and HCl aqueous solutions. Those solutions were used to evaluate the maximum regeneration efficiency of dye (For SF, desorption conditions: dye concentration, 50 ppm; adsorbent dosage, 15 mg/25 mL; contact time, 30 min; temperature, 303 K. For NR, desorption conditions: dye concentration, 100 ppm; adsorbent dosage, 20 mg/25 mL; contact time, 30 min; and temperature, 308 K. For CR, desorption conditions: dye concentration, 100 ppm; adsorbent dosage, 50 mg/25 mL; contact time, 70 min; and temperature, 313 K. For RR2, desorption conditions: dye concentration, 100 ppm; adsorbent dosage, 50 mg/25 mL; contact time, 80 min; and temperature, 308 K). The % desorption was calculated by using Eq. 3 [40],

$$\% \text{Desorption} = \frac{\text{Concentration desorbed mg/L}}{\text{Concentration adsorbed mg/L}} \times 100 \quad (3)$$

2.4 Characterisations

FTIR spectra of Si-MCM-41 material before and after adsorbing dyes were recorded using a Perkin Elmer (Model 1600 FTIR Spectrophotometer) over the range 4000–500 cm^{-1} . KBr pellet method was used for recording the FTIR spectra. The surface morphology of the Si-MCM-41 materials before and after adsorbing dyes were evaluated from the HRXRD obtained from thermal ARL X-ray diffractometer equipped with a $\text{CuK}\alpha$ radiation source and a graphite monochromator. The porous structure characteristics including specific surface area, average pore diameter and pore volume pre and post adsorption of dyes were obtained at 77 K with Nova 3200e (Quantachrome, USA). The surface characteristics of the dye adsorbed Si-MCM-41 material were analysed by using HRTEM (Model- JEM-2100, JEOL, Japan). The surface morphology of the pure material was analysed by using FESEM (Model- FESEM Supra 55, Zeiss, Germany).

3 Results and discussion

3.1 Adsorption of different dyes

Removal of dyes from aqueous solution using an adsorbent is known to depend on the temperature, the solution pH, the equilibrium time of adsorption, the adsorbent dosage and finally the initial concentration of dye solution. Those have been optimised and discussed in detailed in Supplementary material (SM, Section 1). Under alkaline conditions, at higher pH, the electrostatic attraction between negatively charged surface of adsorbent and positively charged adsorbate is enhanced, resulting in higher % of adsorption for both SF and NR. Additionally, for both CR and RR2, the adsorption of dye molecules become reduced because of the repulsive forces among negatively charged groups present in the surface of adsorbent and negatively charged adsorbate molecules [41]. The effects of temperature, contact time, dye concentration and adsorbent dose on % of dyes adsorption have been discussed in SM (Fig. S2–S5).

3.1.1 FTIR spectra

Infrared spectra of Si-MCM-41 before and after adsorbing dyes are demonstrated in Fig. 2. Some well known vibrational modes of the material are visible in all the spectra. Infrared spectrum of calcined Si-MCM-41 (Fig. 2) show a broad band due to associated -OH groups (Si-OH) near 3463 cm^{-1} . The -OH bending mode is present near 1637 cm^{-1} . Asymmetric Si-O-Si stretching occurs at 1085 cm^{-1} . Si-O bending in Si-OH is observed near 970 cm^{-1} . Symmetric Si-O-Si stretching occurs at

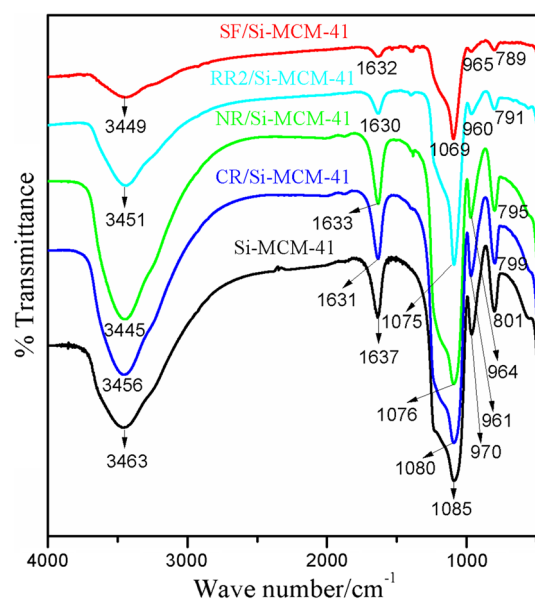


Fig. 2 FTIR spectra of calcined Si-MCM-41 before and after adsorbing dyes; from top to bottom is SF/Si-MCM-41 (pH 9, 50 mg L^{-1} , 303 K), RR2/Si-MCM-41 (pH 2, 100 mg L^{-1} , 308 K), NR/Si-MCM-41 (pH 7, 100 mg L^{-1} , 303 K), CR/Si-MCM-41 (pH 4, 100 mg L^{-1} , 313 K), Si-MCM-41 (calcined). The percentages of the dye to the anion exchange capacity of Si-MCM-41 are 1.296, 1.227, 0.239, and 0.202 meq/g for SF, NR, CR, and RR2 respectively

801 cm^{-1} [42]. But, the dye loaded Si-MCM-41 materials exhibit the characteristic peaks of broad band due to associated -OH groups (Si-OH) near 3449, 3451, 3445 and 3456 cm^{-1} for SF, RR2, NR, and CR respectively. The -OH bending mode shifted to 1632, 1630, 1633 and 1631 cm^{-1} for SF, RR2, NR, and CR respectively. The shifting of -OH bonds indicate H-bonding, because H-bonding lowers the energies of absorption ($E = h\nu$). The asymmetric Si-O-Si stretching shifted to 1069, 1075, 1076 and 1080 cm^{-1} for SF, RR2, NR, and CR respectively. The Si-O bending in Si-OH shifted to 965, 960, 964 and 961 cm^{-1} for SF, RR2, NR, and CR respectively. The symmetric Si-O-Si stretching shifted to 789, 791, 795 and 799 cm^{-1} for SF, RR2, NR, and CR respectively. This suggests that electrostatic as well as H-bonding interaction may involve between the active sites of dyes and -OH groups present on the surface of adsorbent (Fig. S12, SM). Moreover, the characteristic absorption peaks of the Si-MCM-41 in the range between 970 and 960 cm^{-1} are also observed for all samples, which implies that there is no change in the pore structure of Si-MCM-41 after adsorption.

3.1.2 HRXRD analysis

From the HRXRD patterns (Fig. 3) of Si-MCM-41 before and after adsorbing dyes, it is obvious that the presence of

(100), (110), (200) and (210) diffraction peaks in the primary Si-MCM-41 depicts the crystalline nature of the calcined material. Various changes have occurred after the adsorption of dyes onto Si-MCM-41. From Fig. 3, it is observed that not only the disappearance of the major peaks but also peak shifting took place. HRXRD patterns NR/Si-MCM-41 and SF/Si-MCM-41 reveal no peaks due to (100), (110), (200) or (210) diffractions, clearly signifying that the crystalline character of the adsorbent has been suppressed by high adsorption of adsorbates.

3.1.3 Nitrogen adsorption–desorption isotherms

The nitrogen adsorption–desorption isotherms (Fig. 4) were measured to investigate the changes that occurred in the pore structure of Si-MCM-41. Specific surface area, average pore diameter, total pore volume data are given in Table 1. The BET surface area for the calcined material is 973 m²/g and the average pore diameter is 2.42 nm. The total pore volume of the calcined material is 0.758 cm³/g. It is observed that the BET surface area of Si-MCM-41, becomes decreased more effectively for both NR/Si-MCM-41 (47 m²/g) and SF/Si-MCM-41 (66 m²/g) than that of both CR/Si-MCM-41 (337 m²/g) and RR2/Si-MCM-41 (392 m²/g) dyes. Not only BET surface area but also average pore diameter along with total pore volume decreased more effectively for both NR/Si-MCM-41 and SF/Si-MCM-41 compared to both CR/Si-MCM-41 and

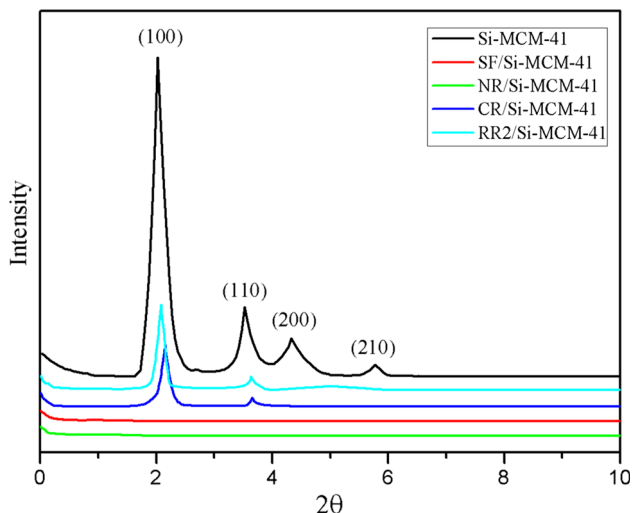


Fig. 3 HRXRD patterns of calcined Si-MCM-41 before and after adsorbing dyes; from top to bottom is calcined Si-MCM-41, SF/Si-MCM-41 (pH 9, 50 mg L⁻¹, 303 K), NR/Si-MCM-41 (pH 7, 100 mg L⁻¹, 303 K), CR/Si-MCM-41 (pH 4, 100 mg L⁻¹, 313 K), RR2/Si-MCM-41 (pH 2, 100 mg L⁻¹, 308 K). The percentages of the dye to the anion exchange capacity of Si-MCM-41 are 1.296, 1.227, 0.239, and 0.202 meq/g for SF, NR, CR, and RR2 respectively

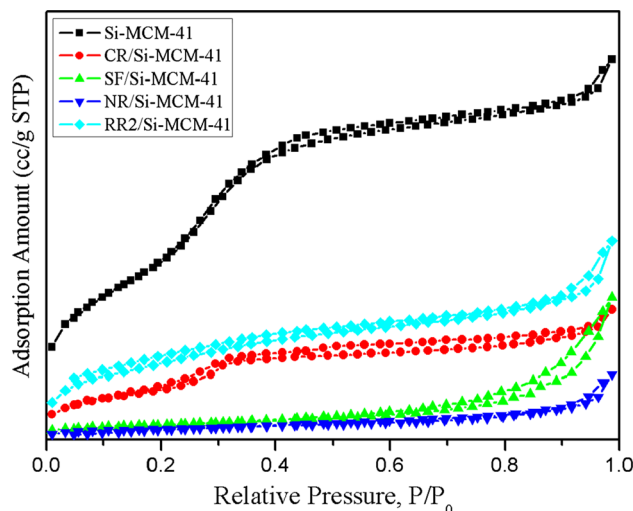


Fig. 4 Nitrogen adsorption–desorption isotherms of Si-MCM-41 (calcined) before and after adsorbing dyes; from top to bottom is Si-MCM-41 (calcined), CR/Si-MCM-41 (pH 4, 100 mg L⁻¹, 313 K), SF/Si-MCM-41 (pH 9, 50 mg L⁻¹, 303 K), NR/Si-MCM-41 (pH 7, 100 mg L⁻¹, 303 K), RR2/Si-MCM-41 (pH 2, 100 mg L⁻¹, 308 K). The percentages of the dye to the anion exchange capacity of Si-MCM-41 are 1.296, 1.227, 0.239, and 0.202 for SF, NR, CR, and RR2 respectively

RR2/Si-MCM-41 dyes. The reason behind this is the surface of Si-MCM-41 was blocked by both NR and SF during the adsorption process and these dyes may screen the surface as well as the pores of the Si-MCM-41 more effectively, which become inaccessible for the nitrogen molecules at the time of analysis. It is observed that the primary Si-MCM-41 (calcined) shows clear capillary condensation at moderate nitrogen pressure. However, after dye adsorption onto Si-MCM-41, the capillary condensation phenomenon becomes insignificant which indicates that the adsorption process may decrease the pore size uniformity and also the specific surface area. The pore sizes can be calculated from the X-ray diffraction interplanar spacing (Fig. 3) and nitrogen isotherms (Fig. 4) using the equation,

$$S = bd \sqrt{\left(\frac{\rho V_p}{1 + \rho V_p}\right)} \tag{4}$$

where *b* is a constant, *S* is the pore size dependent on the assumed pore geometry and is equal to 1.155 for hexagonal models, *V_p* is the mesoporous volume, *ρ* is the pore wall density (i.e. 2.2 cm³/g for siliceous materials), *d* is the XRD interplanar spacing [43]. The average pore diameter of both SF/Si-MCM-41 and NR/Si-MCM-41 are difficult to estimate due to the absence of (100) peak in Fig. 3. So, it is observed that an enormous decrease occurs in specific surface area, average pore diameter and total pore volume of Si-MCM-41 after dye adsorptions.

3.1.4 FESEM and HRTEM analysis

Both FESEM and HRTEM are important tools for characterising the surface morphology as well as fundamental physical properties of the adsorbent surface. It is useful for determining the particle shape, porosity and approximate size distribution of the adsorbent. FESEM and HRTEM images reveal that fine particles have been formed (Fig. 5a, b). Si-MCM-41 has considerable number of pores and there is a good possibility for dyes to be trapped and adsorbed into these pores. After adsorption of dyes (Fig. 5c–f), pores have been covered up (indicated by white arrows).

According to the adsorption efficacy and the analysis of FTIR spectra, HRXRD patterns, nitrogen adsorption–desorption isotherms, FESEM and HRTEM, it is experimentally demonstrated that the adsorption capacity of dyes (especially both of SF and NR) is closely related to the pore structure stability and specific surface area of Si-MCM-41 during the adsorption process.

3.2 Kinetics study

Dye adsorption rate is highly dependent on residence time. During the adsorption process, adsorbate molecules migrate to the outer surface of the adsorbent, diffuse to the

Table 1 BET surface areas, average pore diameter, total pore volume, and sorption conditions of Si MCM-41s before and after absorbing dyes

Material	BET surface area (m ² /g)	Average pore diameter (nm)	Total pore volume (cm ³ /g)	Sorption conditions	Anion exchange capacity (meq/g) (% dye solution)
Si-MCM-41	973	2.42	0.758	–	–
CR/Si-MCM-41	337	1.77	0.296	pH 4, 100 mg L ⁻¹ , 313 K	0.239
SF/Si-MCM-41	66	–	0.139	pH 9, 50 mg L ⁻¹ , 303 K	1.296
NR/Si-MCM-41	47	–	0.116	pH 7, 100 mg L ⁻¹ , 303 K	1.227
RR2/Si-MCM-41	392	1.82	0.309	pH 2, 100 mg L ⁻¹ , 308 K	0.202

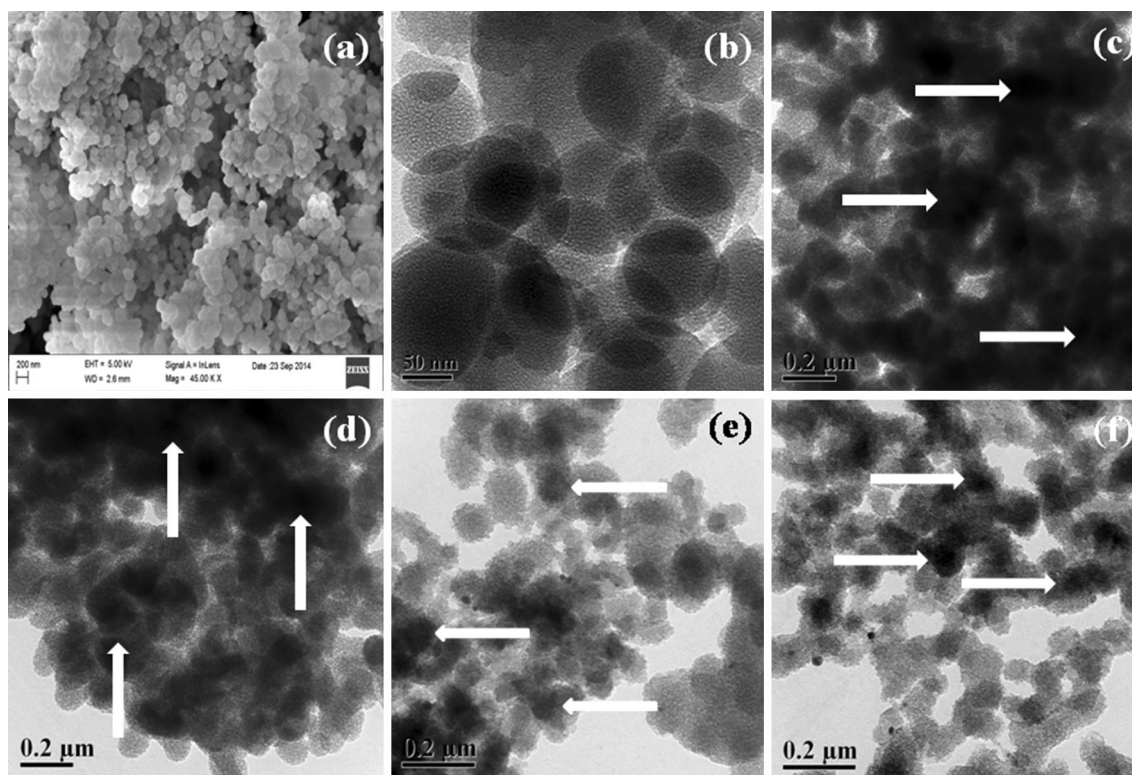


Fig. 5 a FE-SEM image of calcined Si-MCM-41. HR-TEM images of calcined Si-MCM-41 before (b) and after adsorbing dyes such as (c) SF/Si-MCM-41 (pH 9, 50 mg L⁻¹, 303 K), d NR/Si-MCM-41 (pH 7, 100 mg L⁻¹, 303 K), e CR/Si-MCM-41 (pH 4, 100 mg L⁻¹,

313 K), f RR2/Si-MCM-41 (pH 2, 100 mg L⁻¹, 308 K). The percentages of the dye to the anion exchange capacity of Si-MCM-41 are 1.296, 1.227, 0.239, and 0.202 meq/g for SF, NR, CR, and RR2 respectively

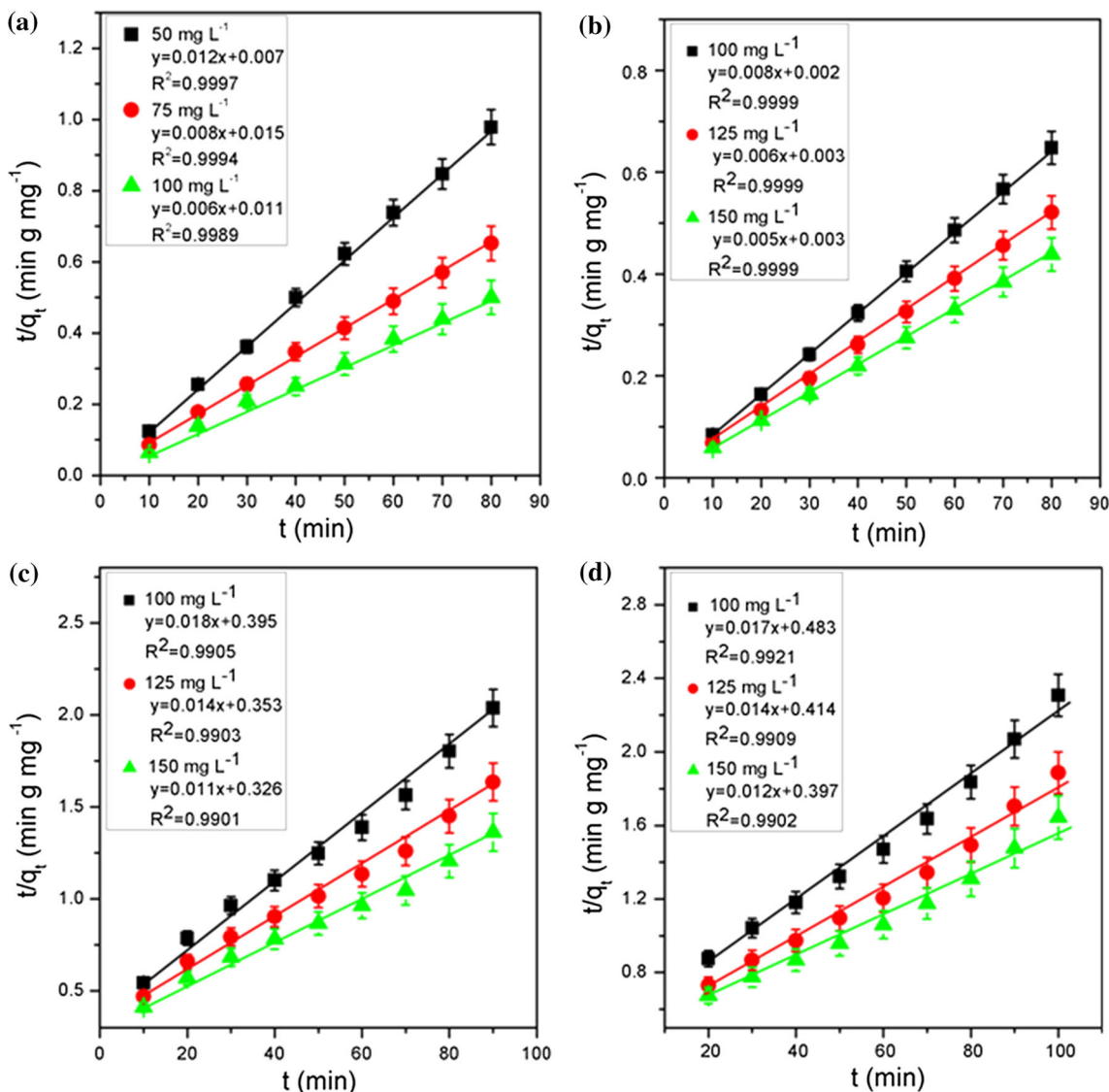


Fig. 6 Modelling of the adsorption kinetics of **a** SF, **b** NR, **c** CR and **d** RR2 using pseudo-second-order model onto Si-MCM-41 as adsorbent

boundary layer and from the particle surface into the internal sites via pore diffusion [38]. To investigate the adsorption process on Si-MCM-41, pseudo-first-order [44], pseudo-second-order [45], second order [46], and intraparticle diffusion [47] kinetics models were used (for details, see SM, Section 2, Fig. S6–S8 and Table S1–S4). From Fig. 6, it is apparent that the kinetics data of dye adsorption using Si-MCM-41 fitted well with pseudo-second-order model which exhibits higher correlation coefficient (R^2) and lower χ^2 value (see SM; Table S1–S4), compared to other models.

Weber and Morris plot was also used to investigate the intraparticle diffusion kinetics model and its mechanism (see SM, Fig. S8). If the plots q_t vs. $t^{1/2}$ is linear and passes through the origin, then intraparticle diffusion is the rate limiting step [48, 49]. However, if the plot does not pass

through the origin, having an intercept (C) which gives an idea about the thickness of the boundary layer. This also indicates that intraparticle diffusion is involved in the adsorption process. Therefore, the presence of multilinearity and the boundary layer thickness suggests that some other mechanism may also play a significant role in the dye uptake process in association with intraparticle diffusion model. Most probably, both surface adsorption and intraparticle diffusion are likely to take place simultaneously.

3.3 Adsorption isotherms

The current research presents a method of direct comparison of the isotherm fit of several models to enable the best-fit and best isotherm parameters to be obtained. Beside this, adsorption isotherm shows how the adsorbate molecules

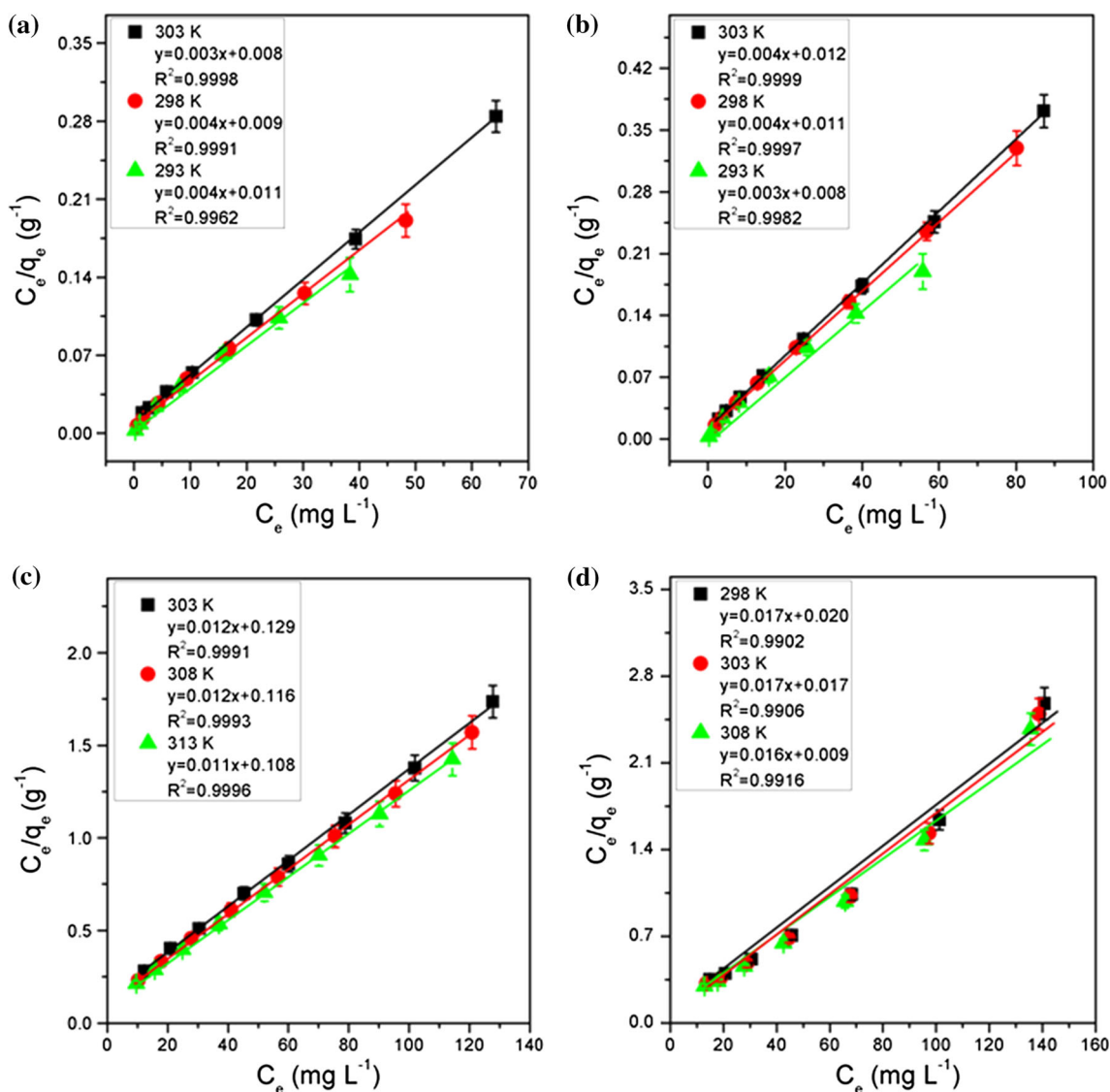


Fig. 7 Modelling of the adsorption isotherms of **a** SF, **b** NR, **c** CR and **d** RR2 using Langmuir model onto Si-MCM-41 as adsorbent

are distributed between the liquid phase and solid phase. Langmuir [50], Freundlich [51], Temkin [52] isotherm models are most frequently used adsorption models and all the models were used to fit the experimental data. The various isotherm models have been explained in SM (see Fig. S9–S10, Table S5–S8).

The essential feature of the Langmuir isotherm can be expressed in terms of a dimensionless factor called separation factor R_L , which is an important characteristics of the Langmuir isotherm model [53].

$$R_L = \left(\frac{1}{1 + bC_0} \right) \quad (5)$$

where C_0 is the initial concentration of corresponding dyes and b is the Langmuir constant. The value of R_L signifies whether the Langmuir model is linear ($R_L = 1$), favourable

($0 < R_L < 1$), irreversible ($R_L = 0$) or unfavourable ($R_L > 1$). The values of R_L are found to be $0 < R_L < 1$, which implies the favourable uptake of these dyes from aqueous solution. It has also been observed that Langmuir isotherm model shows higher correlation coefficient and lower χ^2 value (see SM, Table S5–S8).

It is observed from Fig. 7 that Langmuir isotherm model shows better mathematical fit with experimental data in contrast to Freundlich, and Temkin isotherm models (based on the higher correlation coefficient (R^2) and lower χ^2 value). A basic assumption of Langmuir theory is that sorption takes place at specific sites within the adsorbent. This means that the adsorption of dye takes place at specific homogeneous sites and mono layer adsorption on the surface of Si-MCM-41. Also, investigations carried out at various temperatures suggest that the adsorption is monolayer. From Langmuir

isotherm models at various temperatures (303 K for SF, 303 K for NR, 313 K for CR, and 308 K for RR2), q_m were found to be 275.5, 288.2, 87.4, and 60.2 mg g⁻¹ respectively. This indicates that the Si-MCM-41 is having very high adsorption capacity to remove both of SF and NR dyes from aqueous solution. The values of Langmuir constant ‘ b ’ also increased with temperature. This specifies the stronger affinity between the active sites of the adsorbent and adsorbate molecules [39].

3.4 Thermodynamics study

Thermodynamic studies are important to find out the nature of adsorption process. Thermodynamic parameters were determined using van’t Hoff’s equation, which is given by:

$$\ln b = \frac{\Delta S^\circ}{R} - \frac{\Delta H^\circ}{RT} \quad (6)$$

$$\Delta G^\circ = \Delta H^\circ - T\Delta S^\circ \quad (7)$$

Where ΔG° is the change in Gibbs free energy (J Mol⁻¹), ΔH° is the change in enthalpy (J Mol⁻¹), ΔS° is the change in entropy (J Mol⁻¹ K⁻¹), R is the universal gas constant (8.314 J Mol⁻¹ K⁻¹) and b is the Langmuir gas constant at temperature T (K). The variation in the extent of adsorption with respect to temperature has been explained on the basis of thermodynamic parameters i.e. change in standard free energy, enthalpy and entropy. The values ΔS° and ΔH° (see SM) were evaluated from the intercept and slope of a plot of $\ln b$ versus $1/T$ (Fig. 8). The negative values of ΔG° (see SM) confirms the spontaneous nature of the dye uptake process. It was also observed that with increase in temperature, the values of ΔG° gradually decreased (see SM). This implies stronger adsorptive force, which results in higher degree of spontaneity at higher temperature. The positive values of ΔH° (see SM) suggest that the process is endothermic [54]. The positive values of ΔS° (see SM) suggested higher degree of freedom at the solid–liquid interface during the adsorption of dye molecule on the active site of adsorbent [38, 55–57].

3.5 Regeneration study

The adsorption and desorption characteristics of an adsorbent is very important for its potential application. An efficient adsorbent should possess both high adsorption capacities as well as excellent desorption characteristics, to render the sorbent economically viable. Desorption experiments (see SM, Fig. S11) were performed with different media of pH solutions (pH 2, 7 and 9). Desorption study was repeated three times. For both NR and SF, the maximum % desorption were obtained at pH 2 (97.57 % for NR, 97.65 % for SF) and the minimum % desorption

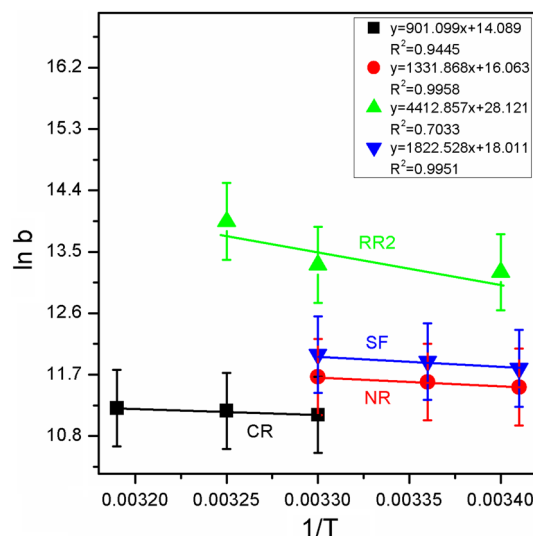


Fig. 8 Thermodynamic study for adsorption of various dyes using Si-MCM-41 as adsorbent; from top to bottom. **a** RR2, **b** SF, **c** NR and **d** CR

were obtained at pH 7 (49.89 % for NR) and at pH 9 (50.36 % for SF). For both RR2 and CR, the maximum % desorption were obtained at pH 9 (86.02 % for RR2, 86.81 % for CR) and the minimum % desorption were obtained at pH 2 (29.33 % for RR2, 31.69 % for CR), which is an opposite trend observed in adsorption (see SM). This provides clear evidence of reusability of the adsorbent for the treatment of respective dyes from aqueous solution and this result also indicates that dyes uptake may follow the ion exchange mechanism [58, 59].

3.6 Adsorption mechanism

It has been observed that various factors play a key role in dye adsorption mechanism, such as the dye structure, textural properties and surface chemistry of adsorbent as well as the specific interaction between the adsorbent surface and adsorbate [60, 61]. In basic and neutral environment, strong electrostatic attraction as well as H-bonding exist between the negatively charged surface of Si-MCM-41 and positively charged groups of the dye molecules, leading to the enhanced adsorption of both SF and NR dyes onto the Si-MCM-41. However, for both CR and RR2, the negatively charged surface of Si-MCM-41 may compete with the anionic dyes, resulting in repulsive forces among the negatively charged adsorbent surface and negatively charged dyes (Fig. S12, SM). The high surface area of Si-MCM-41, also helps to adsorb lower amount of anionic dyes on the Si-MCM-41 surface. Additionally, consecutive diffusion and mass transport process also play an important role in the adsorption process [41, 62–65]. The siloxane

network (Si–O–Si) might be facilitating the mass transport and diffusion process. Thus, it is expected that intraparticle diffusion may also take place and control the dye adsorption process.

4 Conclusions

The present work focused on the plausible effects of interaction among the surface active groups of the dye molecules and Si-MCM-41 on the pore structure of the material and its ability to remove various dyes from aqueous solution. Moreover, all the silica particles can effectively adsorb both SF and NR dyes than CR and RR2 dyes from aqueous solution compared to other adsorbents (Table S13, SI). The electrostatic interactions along with the H-bonding are playing an important role in the adsorption process. The kinetics data follows both pseudo-second-order kinetics and intraparticle diffusion kinetics models simultaneously. The adsorption equilibrium is in good agreement with Langmuir adsorption isotherm, indicating monolayer adsorption on the homogenous surface. Regeneration studies indicate the good regeneration ability of Si-MCM-41. So, based on the data of present investigation, one could conclude that Si-MCM-41 being a proficient adsorbent with high dye adsorption capacity might be a suitable alternative to remove dyes from aqueous solution.

Acknowledgments H.C is thankful to the Director, Indian School of Mines, Dhanbad for providing research fellowship. Authors would like to thank CRF at Indian School of Mines, Dhanbad for providing FESEM facility.

References

1. M.A. Al-Ghouti, M. Khraisheh, S.J. Allen, M.N. Ahmad, The removal of dyes from textile wastewater: a study of the physical characteristics and adsorption mechanisms of diatomaceous earth. *J. Environ. Manage.* **69**, 229–238 (2003)
2. S. Ray, M. Takafuji, H. Ihara, Peptide-based surface modified silica particles: adsorption materials for dye-loaded wastewater treatment. *RSC Adv.* **3**, 23664–23672 (2013)
3. H.A. Mekkawy, M.O. Ali, A.M. El-Zawahry, Toxic effect of synthetic and natural food dyes on renal and hepatic functions in rats. *Toxicol. Lett.* **95**, 155 (1998)
4. C.K. Lee, S.S. Liu, L.C. Jaung, C.C. Wang, K.S. Lin, M.D. Lyu, Application of MCM-41 for dyes removal from wastewater. *J. Hazard. Mater.* **147**, 997–1005 (2007)
5. D. Pokhrel, T. Viraraghavan, Treatment of pulp and paper mill wastewater—a review. *Sci. Total Environ.* **333**, 37–58 (2004)
6. O. Tunay, I. Kabdasli, G. Eremektar, D. Orhon, Color removal from textile wastewaters. *Water Sci. Technol.* **34**, 9–16 (1996)
7. A. Cassano, R. Molinari, M. Romano, E. Drioli, Treatment of aqueous effluents of the leather industry by membrane processes: a review. *J. Membr. Sci.* **181**, 111–126 (2001)
8. K. Srinivasan, M.M. Bhargava, Hepatic binding proteins translocating azo dye carcinogen metabolites from cytoplasm into nucleus in rats. *Food Chem. Toxicol.* **42**, 503–508 (2004)
9. E. Forgacs, T. Cserhati, G. Oros, Removal of synthetic dyes from wastewaters: a review. *Environ. Int.* **30**, 953–971 (2004)
10. G. Crini, Non-conventional low-cost adsorbents for dye removal: a review. *Bioresour. Technol.* **97**, 1061–1085 (2006)
11. E.N. El Qada, S.J. Allen, G.M. Walker, Adsorption of Methylene Blue onto activated carbon produced from steam activated bituminous coal: a study of equilibrium adsorption isotherm. *Chem. Eng. J.* **124**, 103–110 (2006)
12. Z.X. Wu, D.Y. Zhao, Ordered mesoporous materials as adsorbents. *Chem. Commun.* **47**, 3332–3338 (2011)
13. O.G. Rhys, Adsorption on activated carbon—solution to dye waste problems. *J. Soc. Dyers Colour* **94**, 293–297 (1978)
14. K.R. Ramakrishna, T. Viraraghavan, Dye removal using low cost adsorbents. *Water Sci. Technol.* **36**, 189–196 (1997)
15. M. Doğan, M. Alkan, Adsorption kinetics of methyl violet onto perlite. *Chemosphere* **50**, 517–528 (2003)
16. C.C. Wang, L.C. Juang, T.C. Hsu, C.K. Lee, J.F. Lee, F.C. Huang, Adsorption of basic dyes onto montmorillonite. *J. Colloid Interface Sci.* **273**, 80–86 (2004)
17. C. Namasivayam, R.T. Yamuna, Adsorption of direct red 12B by biogas residual slurry: equilibrium and rate processes. *Environ. Pollut.* **89**, 1–7 (1995)
18. S. Netpradit, P. Thiravetyan, S. Towprayoon, Application of ‘waste’ metal hydroxide sludge for adsorption of azo reactive dyes. *Water Res.* **37**, 763–772 (2003)
19. T. Robinson, B. Chandran, P. Nigam, Removal of dyes from an artificial textile dye effluent by two agricultural waste residues, corncob and barley husk. *Environ. Int.* **28**, 29–33 (2002)
20. G. Annadurai, R.S. Juang, D.J. Lee, Use of cellulose-based wastes for adsorption of dyes from aqueous solutions. *J. Hazard. Mater.* **92**, 263–274 (2002)
21. Y. Al-Degs, M.A.M. Khraisheh, S.J. Allen, M.N. Ahmad, Effect of carbon surface chemistry on the removal of reactive dyes from textile effluent. *Water Res.* **34**, 927–935 (2000)
22. A.G. Espantaleon, J.A. Nieto, M. Fernandez, A. Marsal, Use of activated clays in the removal of dyes and surfactants from tannery waste waters. *Appl. Clay Sci.* **24**, 105–110 (2003)
23. J.S. Beck, C. Vartuli, W.J. Roth, M.E. Leonowicz, C.T. Kresge, K.D. Scmitt, C.T.-W. Chu, D.H. Olson, E.W. Sheppard, S.B. McCullen, J.B. Higgins, J.L. Schlenker, A new family of mesoporous molecular sieves prepared with liquid crystal templates. *J. Am. Chem. Soc.* **114**, 10834–10843 (1992)
24. L. Zhou, C. Gao, W. Xu, Magnetic dendritic materials for highly efficient adsorption of dyes and drugs. *ACS Appl. Mater. Interfaces* **2**, 1483–1491 (2010)
25. S. Qadri, A. Ganoe, Y. Haik, Removal and recovery of acridine orange from solutions by use of magnetic nanoparticles. *J. Hazard. Mater.* **169**, 318–323 (2009)
26. A. Afkhami, R. Moosavi, Adsorptive removal of Congo red, a carcinogenic textile dye, from aqueous solutions by maghemite nanoparticles. *J. Hazard. Mater.* **174**, 398–403 (2010)
27. Y. Yu, Y.Y. Zhuang, Z.H. Wang, M.Q. Qiu, Adsorption of water-soluble dyes onto resin NKZ. *Ind. Eng. Chem. Res.* **42**, 6898–6903 (2003)
28. J. Huh, D. Song, Y. Jeon, Sorption of phenol and alkylphenols from aqueous solution onto organically modified montmorillonite and applications of dual-mode sorption model. *Sep. Sci. Technol.* **35**, 243–259 (2000)
29. H. Zhao, K.L. Nagy, Dodecyl sulfate–hydrocalcite nanocomposites for trapping chlorinated organic pollutants in water. *J. Colloid Interface Sci.* **274**, 613–624 (2004)

30. A. Sayari, S. Hamoudi, Y. Yang, Applications of pore-expanded mesoporous silica. 1. Removal of heavy metal cations and organic pollutants from wastewater. *Chem. Mater.* **17**, 212–216 (2005)
31. R. Liu, P. Liao, J. Liu, P. Feng, Responsive polymer-coated mesoporous silica as a pH-sensitive nanocarrier for controlled release. *Langmuir* **27**, 3095–3099 (2011)
32. L.C. Juang, C.C. Wang, C.K. Lee, Adsorption of basic dyes onto MCM-41. *Chemosphere* **64**, 1920–1928 (2006)
33. X.S. Zhao, G.Q. Lu, G.J. Millar, Advances in mesoporous molecular sieve MCM-41. *Ind. Eng. Chem. Res.* **35**, 2075–2090 (1996)
34. J. Wloch, M. Rozwadowski, M. Lezanska, K. Erdmann, Analysis of the pore structure of the MCM-41 materials. *Appl. Surf. Sci.* **191**, 368–374 (2002)
35. N.A. Oladoja, A.K. Akinlabi, Congo red biosorption on palm kernel seed coat. *Ind. Eng. Chem. Res.* **48**, 6188–6196 (2009)
36. S. Chatterjee, M.W. Lee, S.H. Woo, Adsorption of congo red by chitosan hydrogel beads impregnated with carbon nanotubes. *Bioresour. Technol.* **101**, 1800–1806 (2010)
37. Z. Qiao, L. Zhang, M. Guo, Y. Liu, Q. Huo, Synthesis of mesoporous silica nanoparticles via controlled hydrolysis and condensation of silicon alkoxide. *Chem. Mater.* **21**, 3823–3829 (2009)
38. S. Ghorai, A.K. Sarkar, A.B. Panda, S. Pal, Effective removal of Congo red dye from aqueous solution using modified xanthan gum/silica hybrid nanocomposite as adsorbent. *Bioresour. Technol.* **144**, 485–491 (2013)
39. S. Ghorai, A. Sinhamahapatra, A. Sarkar, A.B. Panda, S. Pal, Novel biodegradable nanocomposite based on XG-g-PAM/SiO₂: application of an efficient adsorbent for Pb²⁺ ions from aqueous solution. *Bioresour. Technol.* **119**, 181–190 (2012)
40. M.S. Sajab, C.H. Chia, S. Zakaria, S.M. Jani, M.K. Ayob, K.L. Chee, P.S. Khiew, W.S. Chiu, Citric acid modified kenaf core fibres for removal of methylene blue from aqueous solution. *Bioresour. Technol.* **102**, 7237–7243 (2011)
41. G. Crini, H.N. Peindy, F. Gimbert, C. Robert, Removal of C.I. basic green 4 (malachite green) from aqueous solutions by adsorption using cyclodextrin-based adsorbent: kinetic and equilibrium studies. *Sep. Purif. Technol.* **53**, 97–110 (2007)
42. G. Gu, P.P. Ong, C. Chu, Thermal stability of mesoporous silica molecular sieve. *J. Phys. Chem. Solids* **60**, 943–947 (1999)
43. M. Kruk, M. Jaroniec, A. Sayari, Structural and surface properties of siliceous and titanium-modified HMS molecular sieves. *Micropor. Mater.* **9**, 173–182 (1997)
44. S. Legergren, About the theory of so-called adsorption of soluble substances. *K. Sven. Vetenskapsakad. Handl.* **24**, 1–39 (1898)
45. Y.S. Ho, G. McKay, Pseudo-second order model for sorption processes. *Process Biochem.* **34**, 451–465 (1999)
46. Y.S. Ho, Second-order kinetic model for the sorption of cadmium onto tree fern: a comparison of linear and non-linear methods. *Water Res.* **40**, 119–125 (2006)
47. W.J. Weber, J.C. Morris, Kinetics of adsorption on carbon from solution. *J. San. Eng. Div. ASCE* **89**, 31–59 (1963)
48. A. Ozcan, A.S. Ozcan, Adsorption of acid red 57 from aqueous solutions onto surfactant-modified sepiolite. *J. Hazard. Mater.* **125**, 252–259 (2005)
49. L. Ai, C. Zhang, L. Meng, Adsorption of methyl orange from aqueous solution on hydrothermal synthesized Mg–Al layered double hydroxide. *J. Chem. Eng. Data* **56**, 4217–4225 (2011)
50. I. Langmuir, The constitution and fundamental properties of solids and liquids. *J. Am. Chem. Soc.* **38**, 2221–2295 (1916)
51. H.M.F. Freundlich, Uber die adsorption in Losungen. *Z. Phys. Chem.* **57**, 385–470 (1906)
52. M.J. Temkin, V. Pyzhev, Recent modifications to Langmuir isotherms. *Acta. Physicochem.* **12**, 217–222 (1940)
53. M.M. Ayad, A.A. El-Nasr, Adsorption of cationic dye (methylene blue) from water using polyaniline nanotubes base. *J. Phys. Chem. C* **114**, 14377–14383 (2010)
54. S. Chowdhury, R. Mishra, P. Saha, P. Kushwaha, Adsorption thermodynamics, kinetics and isosteric heat of adsorption of Malachite green onto chemically modified rice husk. *Desalination* **265**, 159–168 (2011)
55. X.F. Sun, S.G. Wang, X.W. Liu, W.X. Gong, N. Bao, B.Y. Gao, H.Y. Zhang, Biosorption of malachite green from aqueous solutions onto aerobic granules: kinetic and equilibrium studies. *Bioresour. Technol.* **99**, 3475–3483 (2008)
56. Y. Zhou, M. Zhang, X. Hu, X. Wang, J. Niu, T. Ma, Adsorption of cationic dyes on a cellulose-based multicarboxyl adsorbent. *J. Chem. Eng. Data* **58**, 413–421 (2013)
57. S. Ghorai, A. Sarkar, M. Raoufi, A.B. Panda, H. Schonherr, S. Pal, Enhanced removal of methylene blue and methyl violet dyes from aqueous solution using a nanocomposite of hydrolyzed polyacrylamide grafted xanthan gum and incorporated nanosilica. *ACS Appl. Mater. Interfaces* **6**, 4766–4777 (2014)
58. I.D. Mall, V.C. Srivastava, G.V.A. Kumar, I.M. Mishra, Characterization and utilization of mesoporous fertilizer plant waste carbon for adsorptive removal of dyes from aqueous solution, colloids and surfaces A: physicochem. Eng. Aspects **278**, 175–187 (2006)
59. A. Roy, S. Chakraborty, S.P. Kundu, B. Adhikari, S.B. Majumder, Lignocellulosic jute fiber as a bioadsorbent for the removal of azo dye from its aqueous solution: batch and column studies. *J. Appl. Poly. Sci.* **129**, 15–27 (2013)
60. R.S. Blackburn, Natural polysaccharides and their interactions with dye molecules: applications in effluent treatment. *Environ. Sci. Technol.* **38**, 4905–4909 (2004)
61. G.Z. Kyzas, M. Kostoglou, N.K. Lazaridis, Relating interactions of dye molecules with chitosan to adsorption kinetic data. *Langmuir* **26**, 9617–9626 (2010)
62. H. Chaudhuri, S. Dash, A. Sarkar, Synthesis and use of SBA-15 adsorbent for dye-loaded wastewater treatment. *J. Environ. Chem. Eng.* **3**, 2866–2874 (2015)
63. N.M. Mahmoodi, Equilibrium kinetics and thermodynamics of dye removal using alginate in binary systems. *J. Chem. Eng. Data* **56**, 2802–2811 (2011)
64. C.P. Sekhar, S. Kalidhasan, V. Rajesh, N. Rajesh, Bio-polymer adsorbent for the removal of malachite green from aqueous solution. *Chemosphere* **77**, 842–847 (2009)
65. H. Chaudhuri, S. Dash, S. Ghoari, S. Pal, A. Sarkar, SBA-16: application for the removal of neutral, cationic, and anionic dyes from aqueous medium. *J. Environ. Chem. Eng.* **4**, 157–166 (2016)